

Strong laser-field effects in hydrogen: High-order above-threshold ionization and photoelectron angular distributions

S. Dionissopoulou, Th. Mercouris, A. Lyras,* and C. A. Nicolaides†

Theoretical and Physical Chemistry Institute, National Hellenic Research Foundation, Vasileos Constantinou 48 Avenue, 116 35 Athens, Greece

(Received 5 December 1996)

The problem of the interaction of the hydrogen atom with a strong laser pulse has been tackled by solving the time-dependent Schrödinger equation via the state-specific expansion approach [Th. Mercouris *et al.*, Phys. Rev. A **50**, 4109 (1994)]. We present above-threshold ionization (ATI) spectra and study the frequency ($\hbar\omega_{\text{laser}}=2-4$ eV) and intensity ($I_0\leq 2\times 10^{14}$ W cm⁻²) dependence of the plateaulike structure appearing at high photoelectron energies. Our findings are qualitatively consistent with experimental data recently obtained in rare gases and render support to the proposed tunneling-rescattering mechanism for the interpretation of the observed features. Additional information on the dynamics of the laser-atom interaction is obtained by studying the frequency and intensity dependence of the photoelectron angular distributions (PADs). In agreement with recent experimental discoveries in rare gases, an appreciable sidelobe structure is found in PADs corresponding to high-order ATI peaks, for low laser frequencies ($\hbar\omega_{\text{laser}}\leq 3$ eV). The connection of the sidelobe structure in the PADs to the ATI plateau is explored and evidence for a common underlying mechanism is produced. Our results suggest that the electron tunneling-rescattering mechanism is not the only one contributing to the appearance of the sidelobe structure in the PADs and the formation of the ATI plateau. [S1050-2947(97)02606-1]

PACS number(s): 42.50.Hz, 32.80.Rm

I. INTRODUCTION

The study of the interaction of strong, short laser pulses with atomic systems has revealed a whole different class of phenomena, prominent among them being the one called above-threshold ionization (ATI) [1], whereby an atom absorbs more photons than the minimum number necessary for ionization, thus giving rise to a series of peaks separated by the photon energy in the photoelectron energy spectra. In recent years, substantial help in the effort of understanding the underlying dynamics of ATI has been provided by measuring the photoelectron angular distributions (PADs). For laser light linearly polarized, the PADs were found to peak along the polarization axis as the order of the ATI peak increased, a trend consistent with a propensity rule in dipole transitions that favors higher-angular-momentum states as the number of absorbed photons increases [2]. However, recent experimental findings shook the validity of this simple picture and revealed another degree of complexity in the ATI dynamics [3–5]. In one set of experiments, Xe and Kr atoms were irradiated by 50-ps, 1.05- μm linearly polarized laser pulses and the recorded PADs exhibited narrow lobes at approximately 45° off the polarization axis in a certain energy range of the ATI spectrum [3]. Subsequent experiments, also with rare gases, utilizing 40-fs, 630-nm linearly polarized laser pulses at intensities up to 4.4×10^{14} W cm⁻² and at repetition rates as high as 6.2 kHz, recorded ATI spectra

exhibiting a substantial change in the slope of the envelope of the peak heights above a certain photoelectron energy [4]. Moreover, in Ar and Xe for sufficiently high laser intensities, a clear plateau in the ATI spectra was observed [4]. The study of the corresponding PADs revealed an appreciable sidelobe structure for a limited range of photoelectron energies, in qualitative agreement with the earlier findings [3].

Although the experiments were performed with rare gases, calculations based on one-dimensional models and on the hydrogen atom [4] as well as on the single-active-electron approximation to the description of the closed-shell noble gases [3] produced results in general qualitative agreement with some of the observations. This fact suggested that the different features are caused mainly by single-electron dynamics with the following interpretation [6,7]. Electrons released with nearly zero kinetic energy through tunneling are subsequently accelerated by the strong electric field of the laser towards the ionic core from which they are rescattered. This rescattering process can be responsible both for the high kinetic energies of the electrons at the plateau of the ATI spectra and for the substantial sidelobe structure of the corresponding PADs, as even purely classical mechanical calculations seem to show [8].

In view of these experimental results and their preliminary interpretation, we chose to study computationally these phenomena by solving the time-dependent Schrödinger equation (TDSE) for the hydrogen atom, where the effect under investigation results exclusively from the one-electron atomic and interaction operators and is not influenced by multielectron effects. Our study has been comprehensive, involving the wavelength as well as the intensity dependence of both the ATI and the PADs, in an attempt to clarify whether the ATI plateaulike structures are due solely to electrons produced by tunneling that is supposed to dominate at

*Permanent address: Department of Physics, University of Ioannina, P.O. Box 1186, 45110, Greece.

†Also at Physics Department, National Technical University, Athens, Greece.

longer wavelengths and higher field strengths [6,7]. Indeed, our results show that at shorter wavelengths ($\hbar\omega > 3$ eV) and at low field strengths (corresponding to $I_0 \sim 10^{13}$ W cm $^{-2}$) neither an ATI plateau nor a sidelobe structure in the PADs can be found, at least for pulse durations of the order of 30–40 fs. We also wanted to establish the correlation, if any, between the appearance of plateaulike structures in the ATI spectra and the sidelobe structure in the corresponding PADs; if there exists a common underlying mechanism, this correlation is expected to be particularly strong and easier to identify in the theoretical results than in the experimental data, where instrumental artifacts might mask it. Our results indicate that tunneling electrons are the main source of interference effects affecting the recently discovered structure in both the ATI spectra and the PADs. However, the interplay between tunneling and multiphoton effects is rather subtle and it is not easy to disentangle their contribution to the observable quantities, at least for the laser parameters employed in the calculations reported below.

The organization of the paper is as follows. First we briefly review the basic elements of the state-specific expansion approach (SSEA) to the solution of the TDSE. Then we present the results of our calculations in hydrogen, grouped according to the laser frequency. A part of these results has been presented elsewhere [9].

II. STATE-SPECIFIC EXPANSION APPROACH TO THE SOLUTION OF THE TDSE

The direct and rigorous way of obtaining quantitative information on the processes discussed above is to solve the TDSE

$$H(t)\Psi(t) = i \frac{d}{dt} \Psi(t) \quad (1)$$

for an atom initially prepared in one of its bound states, which is subjected to a short and intense laser pulse. Knowledge of the time-dependent wave function $\Psi(t)$ allows the evaluation of the physical quantities of interest.

In this work, the usual electric-dipole approximation was made and the solution of Eq. (1) was achieved via the SSEA [10,11], according to which the form of the sought after $\Psi(t)$ is

$$\Psi(\vec{r}, t) = \sum_{n,l} \alpha_{nl}(t) \Psi_{nl}(\vec{r}) + \sum_l \int_0^\infty b_l(\varepsilon, t) \Psi_l(\vec{r}, \varepsilon) d\varepsilon. \quad (2)$$

$\Psi_{nl}(\vec{r})$ and $\Psi_l(\vec{r}, \varepsilon)$ are the exact bound and scattering hydrogenic eigenfunctions, which are computed and utilized in numerical form. The coefficients $\alpha_{nl}(t)$ and $b_l(\varepsilon, t)$ are obtained from the system of coupled integro-differential equations that emerges when Eq. (2) is combined with Eq. (1).

The SSEA was introduced primarily in order to handle the serious problems of electronic structure, electron correlation, multiple excitations, and single or multichannel continua characterizing polyelectronic atoms and small molecules [10–13]. This was shown to be feasible for two main reasons. The first reason has to do with the fact that by employing wave functions that are compact but optimized for each bound, autoionizing, or scattering state entering in Eq. (2),

according to their electronic structure (for polyelectronic systems there is also an index for the various channels), economical and physically transparent accurate calculations are possible. In the context of the calculations of properties of high-order multiphoton processes, especially useful is the finding that for any atomic spectrum the number of discrete states contributing to the expansion (2) is relatively small and therefore it is the large number of the scattering states of the ionized continuum that dominates this expansion. These states are best represented by numerically obtained energy-normalized functions and this is why in the SSEA [10,11] the problem of the on-energy shell singularity in the matrix elements for the length and velocity forms of the electric-dipole approximation was solved for the general case of numerical functions. The second reason is that it proved possible to solve efficiently systems of tens of thousands of coupled integro-differential equations for sufficiently long times and extended energy ranges in the continuous spectrum so as to now know that convergence is possible even for extreme cases of high intensities [14].

Once the coefficients $\alpha_{nl}(t)$ and $b_l(\varepsilon, t)$ have been computed, the time-dependent probability distribution of an electron in the continuous spectrum is given directly by

$$\frac{dP_\varepsilon(t)}{d\varepsilon} = \sum_l |b_l(\varepsilon, t)|^2, \quad (3)$$

which produces the ATI spectrum. For the computation of the PADs we simply project the electronic state

$$\Psi^- = 4\pi \sqrt{\frac{\pi}{2k}} \sum_l \sum_{m=-l}^l i^l e^{-i\delta_l} Y_{lm}^*(\hat{k}) Y_{lm}(\hat{r}) R_{kl}(r), \quad (4)$$

which is composed of an incoming spherical wave and an outgoing plane wave with phase shift δ_l , on the state-specific wave function (2) and integrate over spatial coordinates. Then the probability distribution of emission of an electron of energy $\varepsilon = \frac{1}{2}k^2$ at the time instant t propagating in the direction \hat{k} is given by

$$\frac{d^2 P_\varepsilon(\hat{k}; t)}{d\hat{k} d\varepsilon} = \left| \sum_l \sum_{m=-l}^l (-i)^l e^{i\delta_l} Y_{lm}(\hat{k}) b_l(\varepsilon, t) \right|^2. \quad (5)$$

In the case of hydrogen initially prepared in its ground state and irradiated by a linearly polarized laser pulse, Eq. (5) takes the simpler form

$$\frac{d^2 P_\varepsilon(\vartheta; t)}{d\vartheta d\varepsilon} = \left| \sum_l (-i)^l e^{i\delta_l} Y_{l0}(\vartheta) b_l(\varepsilon, t) \right|^2, \quad (6)$$

where ϑ is the angle between the polarization axis of the laser field and the direction of the ejected photoelectron and δ_l are the Coulomb phase shifts.

III. RESULTS

According to Eq. (6), the probability distribution of the ejected photoelectron of energy ε , at instant t , propagating at an angle ϑ off the laser field polarization axis, is determined by the square of a sum of terms. These terms consist of

time-dependent probability amplitudes $b_l(\varepsilon, t)$ multiplied by factors depending on the phase shift δ_l of the scattering states. A consequence of the above fact is that the calculation of the PADs depends on the accurate calculation of the probability amplitudes of all accessible final states of different angular momenta for a given energy. A small error in the calculation of a probability amplitude $b_l(\varepsilon, t)$ results in a relatively small error in the ATI spectrum $[\sum_l |b_l(\varepsilon, t)|^2]$, while it may have a significant effect on the PADs. Therefore, using the PADs as the testing ground, the possibility of obtaining accurately the coefficients $b_l(\varepsilon, t)$ constitutes a stringent requirement for the theory and calculation of the time-dependent response of an atom in a short and intense laser pulse.

The above analysis is confirmed by the SSEA calculations in a number of cases. For example, when atomic hydrogen is irradiated by an intense laser pulse ($\hbar\omega = 2$ eV, $I_0 = 2 \times 10^{14}$ W/cm²), its ATI spectrum can be found with very good accuracy if the time-dependent wave function is expanded in terms of scattering states with angular momentum $l \leq 15$. The incorporation of states with higher l has an insignificant effect on the spectrum. On the other hand, the PADs are obtained accurately only after incorporating the exact scattering states with angular momenta up to $l = 25$.

Another point related to the reliable calculation of PADs is the possibility of accurate knowledge of the phase shifts δ_l . In the special case of H (pure Coulomb potential) the δ_l are known analytically. For any other atomic system, one must solve the pertinent scattering equations at each energy.

A. Hydrogen in a laser field of frequency $\hbar\omega = 4$ eV

We consider the hydrogen ground state interacting with a laser field of relatively short wavelength in a range of peak intensities I_0 between 1×10^{13} and 2×10^{14} W/cm². The laser pulse has the form $E(t) = E_0 f(t) \sin(\omega t + \varphi_0)$, with $E_0 \sim \sqrt{I_0}$ the peak field strength, φ_0 the initial phase of the field, ω the frequency of the laser, and $f(t)$ the function that describes the temporal pulse shape with a total length of 37 fs,

$$f(t) = \begin{cases} t/T_r, & 0 \leq t \leq T_r, & T_r = 16 \text{ T} \\ 1, & T_r \leq t \leq T_f, & T_f = 20 \text{ T} \\ \frac{T_0 - t}{T_0 - T_f}, & T_f \leq t \leq T_0, & T_0 = 36 \text{ T}. \end{cases} \quad (7)$$

As we increase the peak intensity I_0 , the ATI spectra extend to larger energies in the continuum. The spectra exhibit a series of well-distinguished peaks, separated by the photon energy $\hbar\omega$. The relative heights of the consecutive peaks decrease as their order (or the number of the absorbed photons) increases. Even in the case of the maximum peak intensity ($I_0 = 2 \times 10^{14}$ W/cm²) the ATI spectrum does not exhibit any plateau structure. The PADs have the same qualitative characteristics for the whole range of intensities between 1×10^{13} and 2×10^{14} W/cm². For the case of maximum intensity, $I_0 = 2 \times 10^{14}$ W/cm², the ATI spectrum is shown in Fig. 1. The PADs corresponding to photoelectrons that have absorbed N photons ($4 \leq N \leq 11$) are depicted in Fig. 2. Their structure is typical since the photoelectron ejection takes place preferentially parallel to the polarization axis

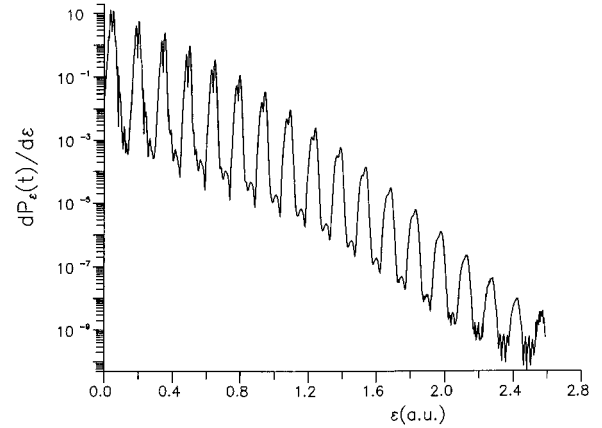


FIG. 1. ATI spectrum of H irradiated by a laser pulse of frequency $\hbar\omega = 4$ eV and peak intensity $I_0 = 2 \times 10^{14}$ W/cm² at the end of the pulse.

of the laser field ($\vartheta = 0, \pi$). This characteristic becomes more pronounced as the energy of the ejected photoelectron increases.

The PADs in Fig. 2 have been obtained from the application of Eq. (6) and have been normalized to unity. They have also been ‘‘symmetrized’’ with respect to the angle $\pi/2$ [15]. In Fig. 3 some of these PADs are shown unnormalized and unsymmetrized.

It is found that these PADs are symmetric with respect to $\pi/2$, with the exception of the second ATI peak, which exhibits a slight but notable asymmetry. The initial state is spherically symmetric and there is no preferred spatial direction in the process. Therefore, the PADs should be symmetric with respect to $\pi/2$, reflecting the underlying symmetry of the angular-momentum selection rules. However, in a numerical simulation, the initial field values do define a preferred direction in space as well as a definite initial phase for the field, conditions that may result in asymmetric PADs. The asymmetry will be more pronounced if the initial field values are large compared to the ground atomic state binding field and/or if the interaction time is not sufficiently long (a few tens of field cycles) for the memory of the initially preferred spatial direction to be averaged out. It is obvious from the above that a remedy to this computational artifact would be either to prolong the total length of the pulse or to increase the turn-on time of the pulse. All of the above would increase significantly the computation time without providing additional insight into the physics of the process. We have chosen a different approach that is both computationally efficient and physically meaningful. We have performed a number of calculations in which the initial phase of the field was either φ_0 or $\pi + \varphi_0$, where φ_0 can be any value in the interval $[0, 2\pi]$. The PADs obtained with initial phase φ_0 were the exact mirror image with respect to $\pi/2$ of those obtained with initial phase $\pi + \varphi_0$. Therefore, the PAD obtained by averaging the two results calculated with initial phases differing by π would be completely symmetric and would reflect the realistic situation of an experimental result obtained by averaging over a large number of laser shots with uniformly distributed random initial phases. Once it was confirmed in worst-case-scenario calculations (high peak intensity and steep pulse turn-on) that the symmetrization pro-

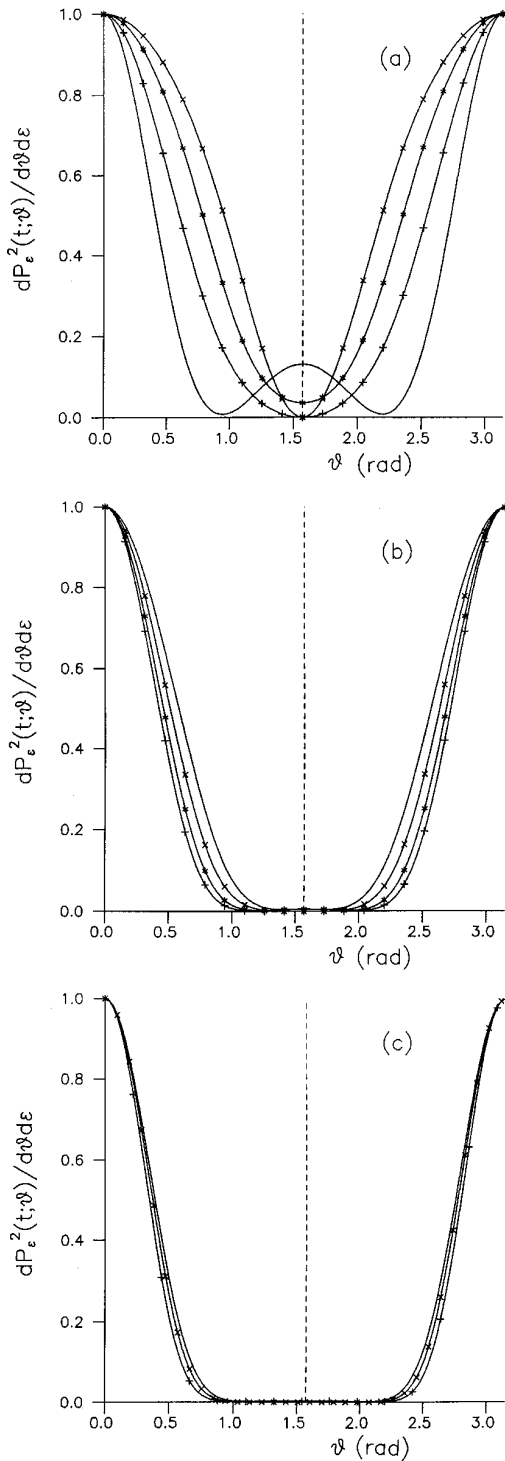


FIG. 2. Angular distributions of photoelectrons corresponding to the ATI spectrum peaks of Fig. 1 as follows: (a) —, first; —×—×, second; —*—*, third; —+—+, fourth. (b) —, fifth; —×—×, sixth; —*—*, seventh; —+—+, eighth. (c) —, ninth; —×—×, tenth; —+—+, eleventh. These PADs have been normalized to unity and have also been “symmetrized” with respect to the angle $\pi/2$.

cedure was valid, we resorted to the computationally economic approach of calculating one PAD with zero initial phase and then appropriately symmetrizing it with respect to $\pi/2$. This situation is particularly relevant to the recently

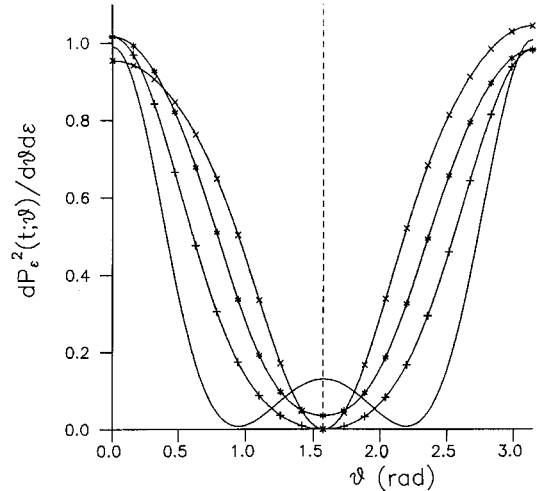


FIG. 3. Same as in Fig. 2(a), but before normalization and symmetrization.

introduced 25 fs [full width at half maximum (FWHM)] laser pulses, while for longer pulses (on the order of 100 fs FWHM) the long tails of the pulse provide sufficient time for any initial phase memory to be averaged out.

The probability distribution over the partial waves at the end of the pulse, for a photoelectron of energy ε , shows that the selection rules are followed (Fig. 4). For the emission of a photoelectron after the absorption of an odd number of photons [e.g., the tenth peak in Fig. 4(b)] the odd partial waves are dominant (the initial state is $1s$). On the other hand, the absorption of an even number of photons [the ninth peak in Fig. 4(a)] results in the excitation of predominantly even partial waves. The opposite symmetry partial waves in both cases have a nonzero excitation probability. The mixing of even and odd partial waves is a natural consequence of the initially preferred spatial direction defined by the field that breaks the spatial isotropy and spherical symmetry of the system and is directly related to any asymmetry with respect to $\pi/2$ observed in the PADs. An alternative way of looking at the numerical results is to invoke the large Fourier bandwidth of our very short pulse that contains a broad range of frequencies around the fundamental, some of which may have sufficient energy to efficiently induce multiphoton processes of order different from the one corresponding to the absorption of the fundamental frequency, thus exciting partial waves of different symmetry. The two interpretations can be considered complementary to one another, providing equivalent pictures in the time and frequency domains, respectively. In the following subsections we turn to the results of the study of the PADs as a function of the frequency of the laser pulse.

B. Hydrogen in a laser field of frequency $\hbar\omega = 3\text{ eV}$

Consider hydrogen in an intense ($I_0 = 2 \times 10^{14}\text{ W/cm}^2$) laser field of frequency $\hbar\omega = 3\text{ eV}$. This smaller frequency increases the order of multiphoton processes and the probability of tunneling. This may drive the system to exhibit structures in the ATI spectrum or in the PADs, which, in the previous case, were absent. For reasons of analogy to the

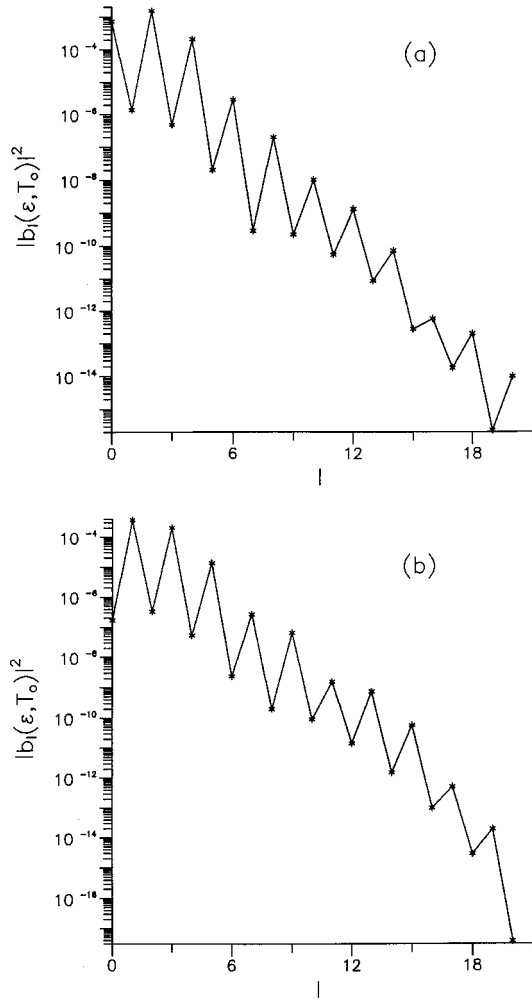


FIG. 4. Probability distribution to the partial waves $|b_l(\varepsilon, T_0)|^2$ of the photoelectrons corresponding to the (a) ninth peak and (b) tenth peak of the ATI spectrum of Fig. 1.

previous application with $\hbar\omega = 4$ eV, we chose the pulse shape of Eq. (7), but for $T_r = 8$ T, $T_f = 10$ T, and $T_0 = 18$ T.

The above conditions lead to an ionization potential of 0.62 a.u. and a ponderomotive potential 0.118 a.u. for the peak intensity. So the minimum number of photons required for ionization is 6, while for the unperturbed atom it would have been 5. The Keldysh parameter γ takes the value 1.46, suggesting that the multiphoton processes may be the dominant ionization mechanism. However, for such a value of γ , the tunneling probability might still be non-negligible, especially when the laser pulse intensity reaches its peak value.

Convergent results were obtained by expanding $\Psi(t)$ in terms of the exact bound states with $n \leq 20$ and $l \leq 14$ and scattering states with energies $\varepsilon \leq 70$ eV (energy mesh step $\Delta\varepsilon = 0.054$ eV) and $l \leq 20$. The number of coupled integro-differential equations is 27 411. The propagation in time was done with a step equal to 0.238 a.u., resulting in a total number of 4320 time steps.

The ATI spectrum, at the end of the pulse, is shown in Fig. 5. It is characterized by well-distinguished peaks separated by the photon energy $\hbar\omega$. The first few peaks exhibit a complicated structure, which is related to ionization with a

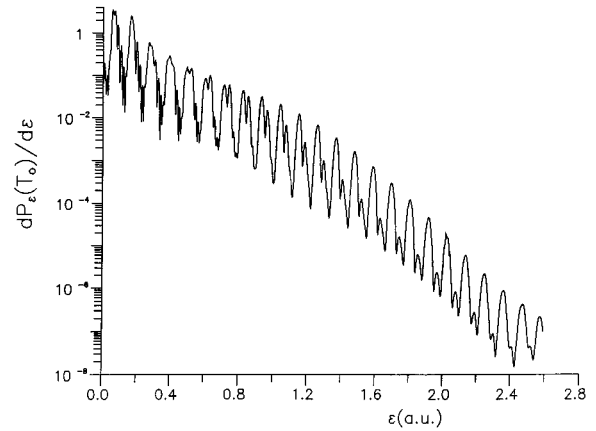


FIG. 5. Same as in Fig. 1, but for frequency $\hbar\omega = 3$ eV and peak intensity $I_0 = 2 \times 10^{14}$ W/cm².

small number of photons from highly excited Rydberg states populated during the rising time of the pulse. For higher photoelectron energies this structure changes to a simpler one. The main peak is accompanied by a second one with decreasing height as the order of the ATI peak is increased. This structure is the result of resonance phenomena between the initial $1s$ state and the states of the $n=3$ shell. Actually, the energy difference between $1s$ and $n=3$ states varies from $4\hbar\omega$ (for intensity $I=0$) to $5\hbar\omega$ (for $I=I_0=2 \times 10^{14}$ W/cm²), as the $3l$ states are shifted to higher energies by an amount equal to the ponderomotive potential $U_p \sim \hbar\omega$. Another important feature of the ATI spectrum is the slow rate of decrease of the heights of the consecutive peaks, in the energy range 0–1.5 a.u., which may be considered as a precursor to a plateau structure. The slope of the envelope of the peak heights is considerably steeper for photoelectron energies above 1.5 a.u.

The PADs for the fifth to the eighth ATI peaks of Fig. 5 are characterized by pronounced sidelobes at angles around 0.75 rad (Fig. 6). The PADs corresponding to the ATI peaks before and after this region are normal (Fig. 7), indicating that for these energies the electron ejection is taking place

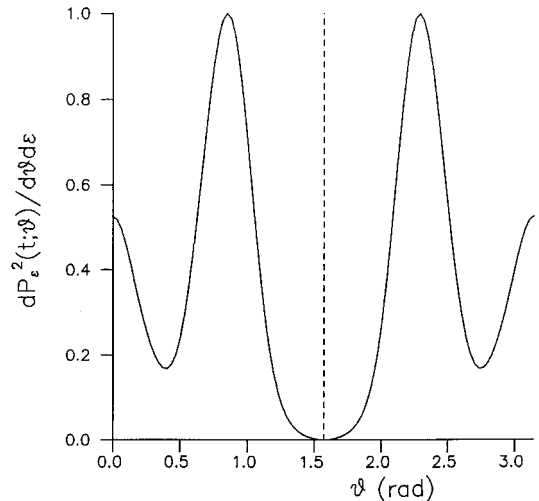


FIG. 6. PAD normalized to unity, corresponding to the sixth ATI peak of Fig. 5.

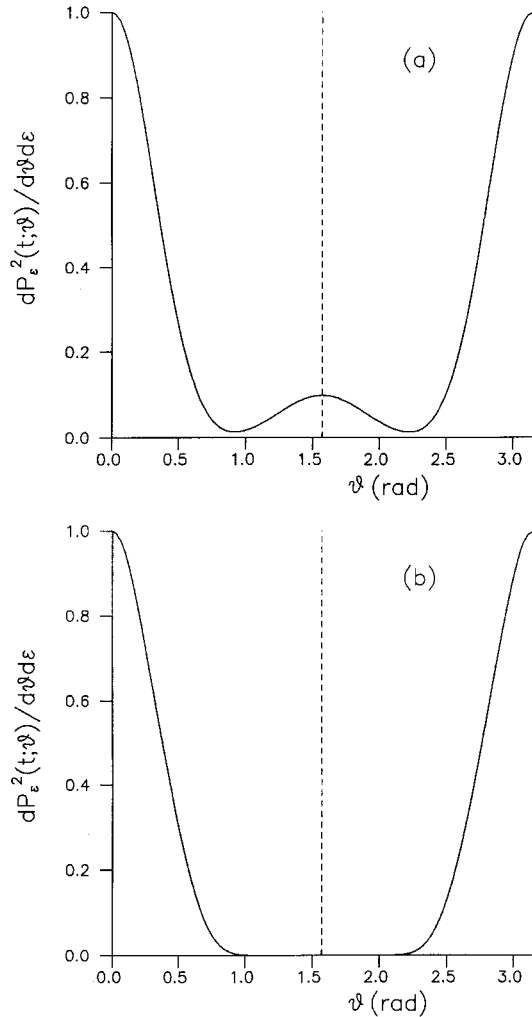


FIG. 7. PADs, normalized to unity, corresponding to the (a) first peak and (b) thirteenth peak of the ATI spectrum of Fig. 5.

mainly along the polarization axis of the laser field. The sidelobes of the PADs, appearing in a certain energy range of the ATI spectrum, are in qualitative agreement with the experimental findings [3]. The significant difference between our results and those of Ref. [3] concerns the energy range of the photoelectrons with sidelobes in their PADs. In fact, the experiment [3] in Xe showed that PADs with sidelobes exist in an energy region around $9U_p$, while in the present case we observe the same structures in the energy range between $4U_p$ and $7U_p$. Thus the suggestion that structured PADs with sidelobes are located at photoelectron energies around $9U_p$ [3] is not generally valid and consequently the semiclassical mechanism of the tunneling electrons rescattered by the nucleus cannot be considered definitive. Obviously, the fully quantum-mechanical behavior is richer than the one accounted for by the current versions of the two-step model.

C. Hydrogen in a laser field of frequency $\hbar\omega = 2$ eV

The previous calculations, for frequencies $\hbar\omega = 3$ and 4 eV showed that the decrease of photon energy, by increasing the order of the multiphoton processes, results in precursors of plateaus in the structure of the ATI spectra and in sidelobes in the corresponding PADs. The simultaneous presence

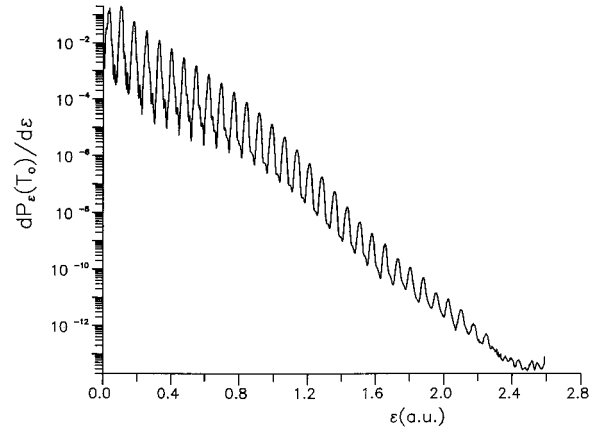


FIG. 8. Same as in Fig. 1, but for frequency $\hbar\omega = 2$ eV and peak intensity $I_0 = 5 \times 10^{13}$ W/cm².

of the two phenomena, in conjunction with their joint absence for the case of the higher frequency $\hbar\omega = 4$ eV, poses the question of the nature of the connection between them. For this reason, we carried out one more set of calculations using short and intense laser pulses of $\hbar\omega = 2$ eV. The pulse shape is the same as in the previous case with $\hbar\omega = 3$ eV.

The ATI characteristics for intensities 5×10^{13} and 2×10^{14} W/cm² have been presented in [17]. For the unperturbed atom, the minimum number of photons required for ionization is 7, while for the intensities 5×10^{13} and 2×10^{14} W/cm² the corresponding numbers of photons are 8 and 11, respectively, since the ponderomotive potential is equal to 0.065 a.u. ($\approx 0.9\omega$) and 0.261 a.u. ($\approx 3.5\omega$), respectively. The Keldysh parameters are 1.96 for the intensity 5×10^{13} W/cm² and 0.98 for 2×10^{14} W/cm². Combined with the results of the calculations, this indicates that for the lower-intensity case the dominant mechanism is multiphoton ionization, while for the higher-intensity case the tunneling mechanism may contribute considerably. The ATI spectrum for laser pulse peak intensity 5×10^{13} W/cm² is shown in Fig. 8. This spectrum is regular, with discrete peaks, without any plateau structure. The PADs for photoelectrons with en-

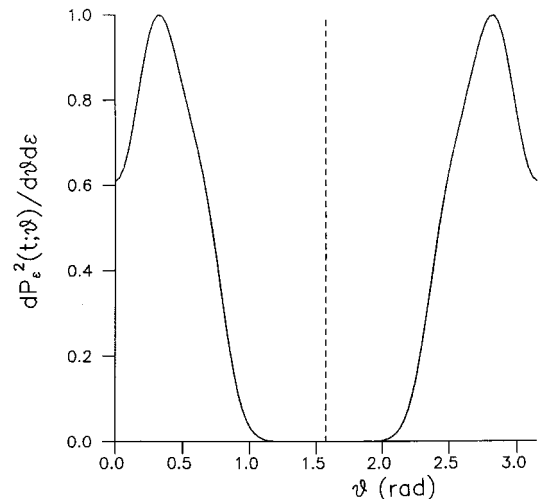


FIG. 9. PAD, normalized to unity, corresponding to the ninth ATI peak of Fig. 8.

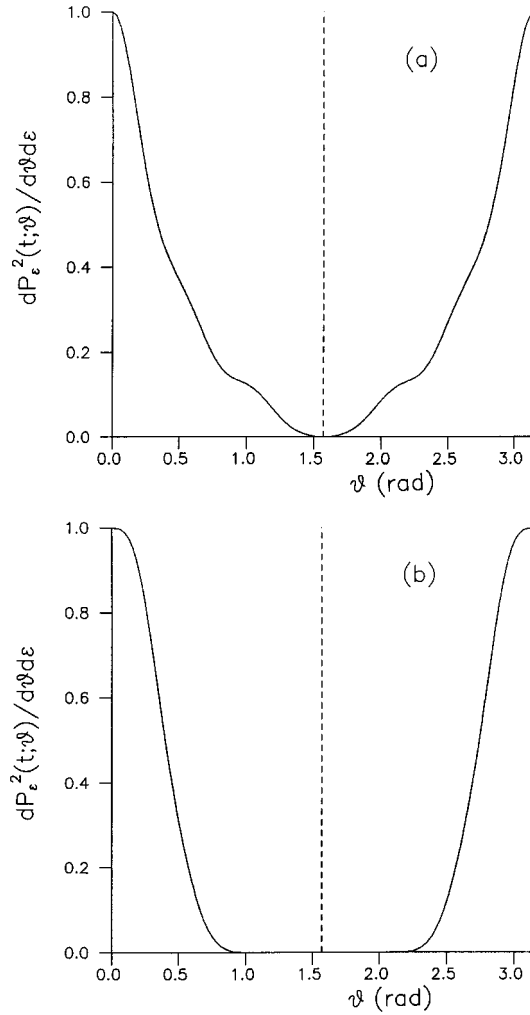


FIG. 10. PADs, normalized to unity, corresponding to the (a) fourth peak and (b) fourteenth peak of the ATI spectrum of Fig. 8.

energies corresponding to the eighth and up to the eleventh ATI peaks are ejected with significant probability at angles 20° with respect to the polarization axis of the laser field (Fig. 9). This energy range is around $9U_p$, in accordance with the experimental findings for rare gases [3]. The photoelectrons with energies out of the range of $9U_p$ show regular PADs (Fig. 10), i.e., emission along the polarization axis of the laser field.

From the probability distributions in the partial waves, corresponding to the ATI peaks shown in Figs. 9 and 10, it was found that the low-angular-momentum partial waves (e.g., for $l=0,2,4,6$) are the most significantly contributing ones, even for peaks that are attributed to multiphoton transitions of order $N=16$ or higher. This suggests that transitions with $\Delta l = +1$ are not favored. The probability of partial waves with $l > N$ is negligible.

Things are more complicated in the case of the high intensity $I_0 = 2 \times 10^{14}$ W/cm 2 . It can be seen from the structure of the ATI spectrum (Fig. 11) that three regions exist. (i) At low energies each ‘‘peak’’ is essentially a group of subpeaks. This dense structure is attributed to transitions from highly excited states with energies shifted up by an amount $\Delta\epsilon$ ($0 \leq \Delta\epsilon \leq U_p = 0.261$ a.u. or, equivalently, $0 \leq \Delta\epsilon \leq 3.5\hbar\omega$). (ii) The peaks from the 7th to the 21st define an extended

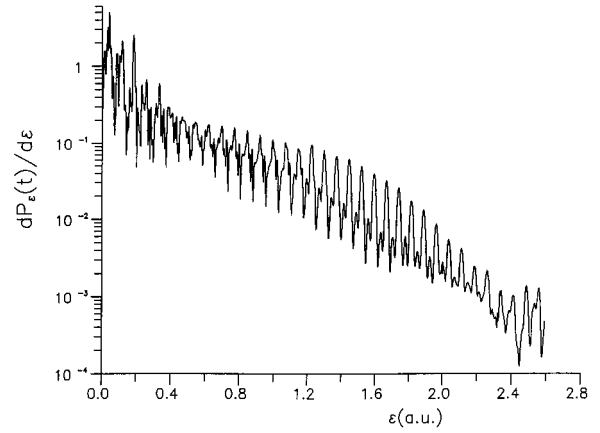


FIG. 11. Same as in Fig. 8, but for peak intensity $I_0 = 2 \times 10^{14}$ W/cm 2 .

plateau. This is in qualitative agreement with the experimental observation of plateaus in the ATI spectrum of H, but for lower intensities [16]. The authors of [16] state that ‘‘it is not possible to compare experiment and theory directly yet’’ since the theory does not take into account the geometrical

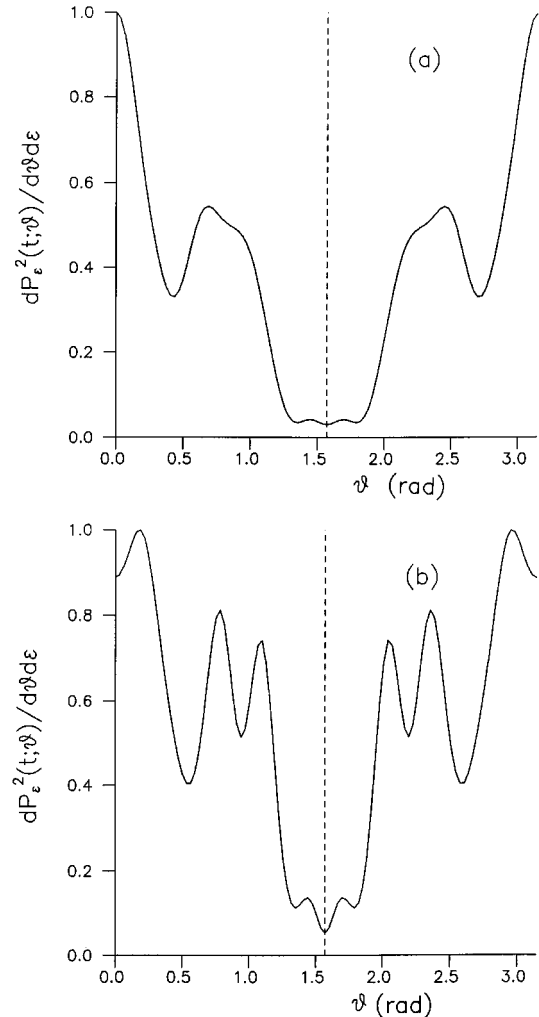


FIG. 12. PADs, normalized to unity, corresponding to the (a) second peak and (b) fourth peak of the ATI spectrum of Fig. 11.

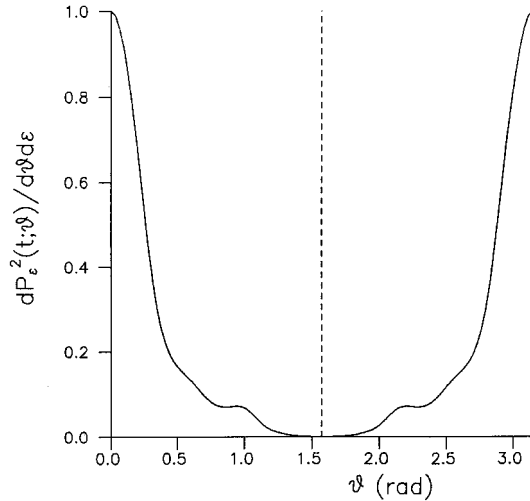


FIG. 13. Same as in Fig. 12, but for the twelfth peak.

properties of the laser focus and the intensity distribution in it, which play an important role in the creation of the observed spectrum. (iii) At high energies the heights of the ATI peaks decrease continuously. The corresponding PADs, at the end of the laser pulse, are grouped into four categories.

(i) The first corresponds to the ATI peaks for low energies ($E < 2U_p$). There the PADs exhibit structures that differ from one peak to the other. For example, in Fig. 12, the PADs for the second and fourth peaks are shown. The number of sidelobes, their positions, and heights are different in each peak. The PADs reflect the mechanism of the transitions that excite the photoelectron to the final state. Some of these spectra [Fig. 12(b)] exhibit nearly isotropic angular distribution.

(ii) The first group of peaks belonging in the ATI plateau has regular PADs. The photoelectron is mainly ejected along the polarization axis of the laser field (Fig. 13).

(iii) The PADs of the ATI peaks from the 17th to the 27th exhibit characteristics similar to those shown in Fig. 14(a), i.e., sidelobes at angles $\vartheta \approx 0.4$ rad.

(iv) Finally, at high photoelectron energies the PADs are again regular, showing emission along the polarization axis of the laser field [Fig. 14(b)].

Summarizing the results for this case ($\hbar\omega = 2$ eV, $I_0 = 2 \times 10^{14}$ W/cm²), a plateau exists in the ATI spectrum (the 7th to the 21st peak), while regularly structured PADs (the 17th to the 27th peak) are found in a limited range of energies. The $9U_p$ scaling [3] is not verified in this calculation. The PADs that exhibit a regular sidelobe structure are nested by a photoelectron energy interval, partly overlapping with the ATI plateau. Therefore, an unambiguous relation between the ATI plateau and the PADs cannot be deduced from the present results, although there is strong evidence pointing to a common underlying mechanism.

The strong perturbation of the atom in conjunction with the short pulse duration results in asymmetric angular distributions with respect to $\pi/2$, at the end of the pulse (Fig. 15). The symmetrization of the PADs is achieved by the process described in Sec. III A. The trapezoidal pulse shape of Eq. (7) [18] “forces” the atom to interact with a rapidly increasing field strength during the rise time of the pulse. In reality,

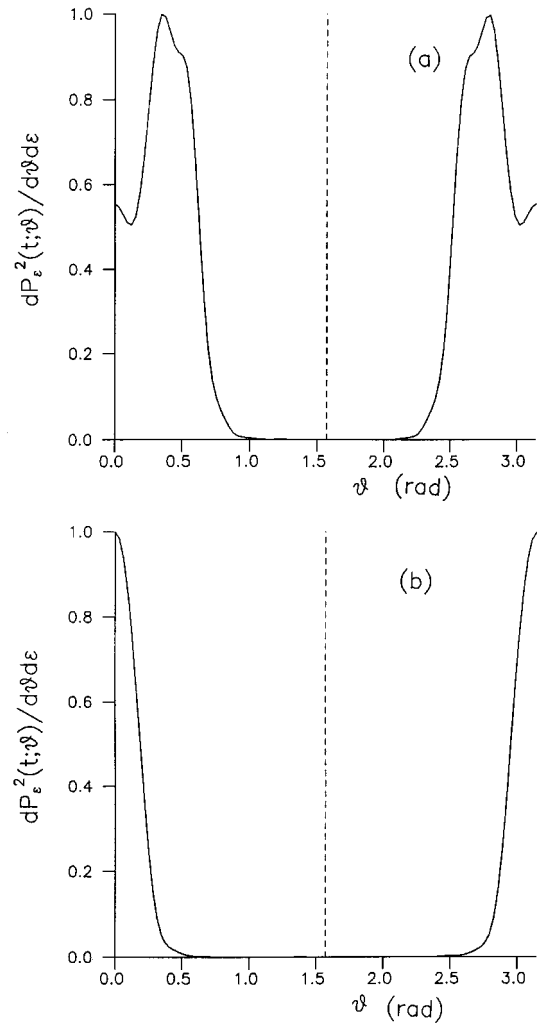


FIG. 14. Same as in Fig. 12, but for the (a) 22nd peak and (b) 34th peak.

the atom probably “feels” a smoother increase of the field strength. For this reason, we carried out a calculation assuming the temporal pulse shape of Fig. 16 (solid line), of 42 T total duration, which is similar to a Gaussian pulse shape of FWHM equal to 18 T (dashed line). The results for the ATI spectrum are shown in Fig. 17. They exhibit the same qualitative characteristics as those of the ATI spectrum in Fig. 11. Although the angular distributions are expected to be more sensitive to the details of the calculation, the comparison of Figs. 18 and 14(a) proves that the qualitative characteristics of PADs remain unchanged, whether the shape is trapezoidal [Eq. (7)] or Gaussian-like (solid line of Fig. 16). In fact, even the quantitative comparison of normalized PADs reveals differences of minor importance.

The strong mixing of even and odd partial waves, found for the ATI peaks in Fig. 17, is reasonable to attribute it to the greater importance of tunneling ionization at lower photon frequencies and higher intensities, a mechanism that is not restricted by angular-momentum selection rules. In addition to this, the number of photons required to ionize the system at certain continuum energies may depend on the time during which ionization occurs, thereby contributing to the mixing of the partial waves because of the different or-

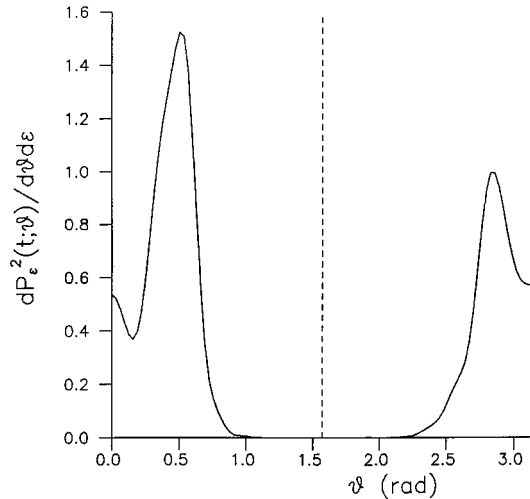


FIG. 15. PAD corresponding to the 22nd peak of the ATI spectrum of Fig. 11, before symmetrization and normalization to unity.

ders of the corresponding multiphoton processes.

IV. CONCLUDING REMARKS

By applying the SSEA to the solution of the TDSE, we produced reliable results for the response (ATI plus PADS) of hydrogen to intense short laser pulses, with frequencies ranging from 2 to 4 eV. Recent experimental spectra [16] concern high-order ATI of hydrogen in intense ultrashort laser pulses of frequency 2 eV. Unfortunately, due to the strong effect of the geometrical properties of the laser focus, the comparisons between experimental findings and theoretical results can be made only qualitatively. Future theoretical work might deal with this problem explicitly.

Our study of the frequency ($\hbar\omega = 2-4$ eV) and intensity ($I \leq 2 \times 10^{14}$ W/cm²) dependence of the ATI spectra and of the corresponding PADS showed the following.

(i) For the smaller frequency $\hbar\omega = 2$ eV and for intensity

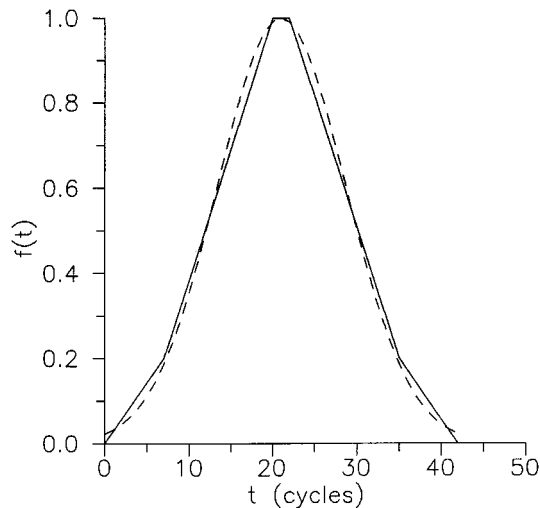


FIG. 16. Piecewise linear temporal pulse shape (solid line) of 42 T total duration approximating a Gaussian pulse shape of 18 T FWHM (dashed line).

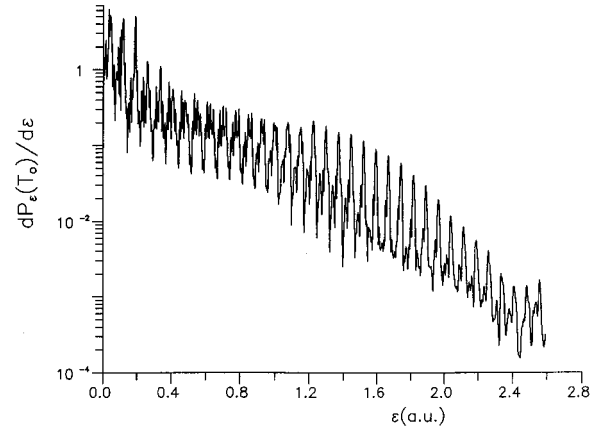


FIG. 17. ATI spectrum of H irradiated by a laser pulse of frequency $\hbar\omega = 2$ eV and peak intensity $I_0 = 2 \times 10^{14}$ W/cm² (as in Fig. 11) at the end of the Gaussian-like pulse shown by a solid line in Fig. 16.

2×10^{14} W/cm², the ATI spectrum exhibits a plateau structure, while for the frequency $\hbar\omega = 3$ eV only a change in the slope of the envelope of the ATI peak heights was found. The ATI spectrum is regular for $\hbar\omega = 4$ eV regardless of the value of the laser pulse peak intensity.

(ii) The PADS exhibit a variety of structures depending on the laser frequency and the field intensity. In the high-frequency case ($\hbar\omega = 4$ eV), the PADS are regular, with the photoelectrons ejected mainly along the polarization axis of the laser field. On the other hand, for the case of $\hbar\omega = 3$ eV and peak intensity 2×10^{14} W/cm², the PADS are regular except for a small energy range ($4-7 U_p$) in the ATI spectrum where the photoelectrons are emitted with appreciable probability at angles 42° with respect to the polarization axis of the laser field. The most interesting case, as far as structure in the PADS is concerned, is for frequency $\hbar\omega = 2$ eV. For the lower peak intensity $I_0 = 5 \times 10^{13}$ W/cm², PADS with sidelobes are present in an energy region around $9 U_p$ in the ATI spectrum. Additionally, for the higher peak

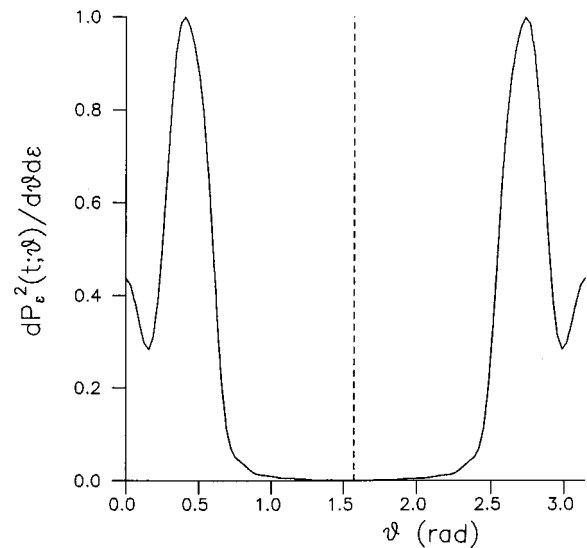


FIG. 18. PADS corresponding to the 22nd ATI peak of Fig. 17.

intensity ($I_0=2\times 10^{14}$ W/cm²) examined in this paper, the PADs are grouped into four categories according to their structure and the energy region to which they belong within the ATI spectrum. The region in the ATI spectrum where sidelobes in the angular distributions of the photoelectrons appear first is located around $6U_p$.

The correlation between these two phenomena—plateaus in the ATI spectrum and sidelobes in the PADs—is subtle because of the different mechanisms that contribute to their formation. Multiphoton processes of high-order produced by short intense pulses of medium frequency ($\hbar\omega=3$ eV) may drive hydrogen to exhibit sidelobes in the PADs in the energy region $4-7 U_p$, which is different from the energy region around $9U_p$ predicted by the “tunneling plus rescattering” mechanism. On the other hand, for the lower-frequency case $\hbar\omega=2$ eV, which favors the tunneling and rescattering

mechanism, we observe that for peak intensity 5×10^{13} W/cm², the sidelobes in the PADs are located at an energy region around $9U_p$ in accordance with the experimental findings for rare gases [3]. The increase of the peak intensity to 2×10^{14} W/cm² results in a variety of structures in the PADs with the region of angular distributions with sidelobes located around $6U_p$. This means that the “rule” of $9U_p$ scaling proposed in [3] for the appearance of sidelobes in the PADs cannot be applied generally since this appearance is controlled by the interference of the multiphoton mechanism with the tunneling plus rescattering one.

ACKNOWLEDGMENT

This work was partly supported by EU Contracts Nos. 93-0242 and 94-0561.

-
- [1] H. G. Muller, P. Agostini, and G. Petite, in *Atoms in Intense Laser Fields*, edited by M. Gavrilu (Academic, London, 1992), p. 1, and references therein.
- [2] H. Rottke, B. Wolf, M. Brichwedde, D. Feldmann, and K. H. Welge, *Phys. Rev. Lett.* **64**, 404 (1990).
- [3] B. Yang, K. J. Schafer, B. Walker, K. C. Kulander, P. Agostini, and L. F. DiMauro, *Phys. Rev. Lett.* **71**, 3770 (1993).
- [4] G. G. Paulus, W. Nicklich, H. Xu, P. Lambropoulos, and H. Walther, *Phys. Rev. Lett.* **72**, 2851 (1994).
- [5] G. G. Paulus, W. Nicklich, and H. Walther, *Europhys. Lett.* **27**, 267 (1994).
- [6] K. J. Schafer, B. Yang, L. F. DiMauro, and K. C. Kulander, *Phys. Rev. Lett.* **70**, 1599 (1993).
- [7] P. B. Corkum, *Phys. Rev. Lett.* **71**, 1994 (1993).
- [8] G. G. Paulus, W. Becker, W. Nicklich, and H. Walter, *J. Phys. B* **27**, L703 (1994).
- [9] S. Dionissopoulou, A. Lyras, Th. Mercouris, and C. A. Nicolaides, *J. Phys. B* **28**, L109 (1995); *J. Phys. B* **28**, 4005(E) (1995).
- [10] Th. Mercouris, Y. Komninos, S. Dionissopoulou, and C. A. Nicolaides, *Phys. Rev. A* **50**, 4109 (1994).
- [11] Th. Mercouris, Y. Komninos, S. Dionissopoulou, and C. A. Nicolaides, *J. Phys. B* **29**, L13 (1996).
- [12] C. A. Nicolaides, S. Dionissopoulou, and Th. Mercouris, *J. Phys. B* **29**, 231 (1996).
- [13] I. D. Petsalakis, Th. Mercouris, and C. A. Nicolaides, *Chem. Phys.* **189**, 615 (1994).
- [14] S. Dionissopoulou, Th. Mercouris, and C. A. Nicolaides, *J. Phys. B* **29**, 4787 (1996).
- [15] K. J. LaGattuta, *Phys. Rev. A* **41**, 5110 (1990).
- [16] G. G. Paulus, W. Nicklich, F. Zacher, P. Lambropoulos, and H. Walter, *J. Phys. B* **29**, L249 (1996).
- [17] S. Dionissopoulou, Th. Mercouris, A. Lyras, Y. Komninos, and C. A. Nicolaides, *Phys. Rev. A* **51**, 3104 (1995).
- [18] The trapezoidal temporal pulse shape permits the direct application of the Taylor-series expansion method (TSEM) [10] for the solution of the TDSE. The TSEM method is approximately 15 times faster than any other we have tried so far for the solution of the TDSE, permitting the completion of such calculations within reasonable times.